Valeology: International Journal of Medical Anthropology and Bioethics (ISSN 2995-4924) VOLUME 02 ISSUE 08, 2024

OPTIMIZATION OF STRUCTURAL AND OPTICAL PROPERTIES IN CU_{1-x}NI_xO COMPOSITE THIN FILMS VIA SPIN COATING

Zaidoon Kadhim Dhiab, Najat A.Dahham

Iraq, Salah al-Din, University of Tikrit, College of Science, Department of Physics

Abstract:

In this work, copper-nickel oxide (Cu1-xNixO) thin films with varying nickel substitution ratios were prepared using spin coating route. The X-ray diffraction (XRD) results showed that all samples are polycrystalline nanostructure. Increasing substitution ratio led to a gradual convert from monoclinic CuO to the cubic NiO phase. Scanning electron microscopy (SEM) revealed porous structure of CuO film. Nickel addition reduced particle size, increased bonding, and decreased surface porosity. High nickel ratio films exhibited disc-shaped structures with nano dimensions. The EDX analysis indicated the low content of oxygen suggesting oxygen vacancies. FTIR spectroscopy showed characteristic bands for nanocrystalline copper oxide, with nickel substitution resulting in the emergence of broad bands corresponding to Ni-O vibrations. Optical absorption spectroscopy showed the absorption edge around 350 nm for all samples, with high transmittance up to 93% for nickel oxide in the visible range. The optical bandgap increased with nickel substitution from 3.90 eV for pure copper oxide to 3.98 eV for pure nickel oxide. The high transmittance and large surface area of Cu1-xNixO films make them ideal for use in gas sensors, photocatalysts, and as window materials in solar cells applications.

Keywords: Cu-Ni oxide, Structural properties, Optical properties.

Introduction

Introduction

In semiconductor physics, copper oxide has received much attention due to its interesting properties. There are two stable oxides in the copper oxide family, cuprous oxide (Cu₂O) and cupric oxide (CuO) [1]. These oxides have unique physical properties and crystalline structure [2]. CuO has been widely used in many different fields due to its excellent electrochemical capabilities, good thermal stability, ease of fabrication, and abundance of naturally occurring raw materials, especially

in its nanoform, in many applications, including antibacterial [3], gas sensors [1], photoelectrochemical sensors [4], solar cells [4], and catalysis [5].

NiO, on the other hand, is a p-type semiconductor with a wide bandgap of approximately 3.6 to 4.0 eV [6]. It is valued for its excellent electrochemical stability, high transparency in the visible region, and catalytic properties, making it a strong candidate for applications in batteries, and transparent conductive coatings [7].

Because the size and shape of nanoparticles create different qualities than their bulk state, studying the process of crystallization is both theoretical and practical. The physical-chemical characteristics are determined by the manner of nanoparticle growth tendency. the growth of nanoparticles varies based on the conditions and approach used [8]. Several techniques are employed for preparing nanostructures with different properties, and each offering unique advantages, such as chemical vapor deposition, thermal evaporation, sol-gel, electrodeposition, etc [9]. For depositing CuO thin films, These deposition techniques provide diverse options for fabricating cupric oxide thin films, allowing researchers to modify film properties for specific applications [10].

Combining two metal oxides, such as CuO and NiO, to form composites at different ratios binds the advantages of both oxides more effectively than their individual forms [11]. This compositional tuning allows for the optimization of the structural, optical, and electronic properties of the resulting films, making them more efficient for a wider range of applications [12]. By adjusting the composition ratio, the optical bandgap of the composite can be precisely controlled, enhancing performance in applications such as photovoltaic cells and optical sensors [13]. The presence of both metal sites creates more active sites for catalytic reactions, improving efficiency in catalytic applications [14].

Given these benefits, metal oxide composites are promising candidates for a variety of applications. In gas sensors, the improved sensitivity and selectivity due to the increased surface area and enhanced catalytic activity make these composites ideal for detecting gases [15]. In photovoltaic cells, the tunable bandgap and transparency combined with the conductive properties can enhance the efficiency of solar cells [16]. In photocatalysis, the large surface area and enhanced catalytic properties make these composites highly effective for applications such as water purification and pollutant degradation [17].

In this work, the structural properties, surface morphology, and optical properties of the prepared $Cu_{1-x}Ni_xO$ composite thin films at different ratios, produced by the spin coating technique, were investigated.

Methods

Material

Copper nitrate (Cu(NO₃)₂.3H₂O) and Nickel nitrate hexahydrate Ni(NO₃)₂·6 H₂O of 99.9% purity, provided by Sigma-Aldrich company, were used as started material.

Samples preparation

Aqueous solutions of Cu(NO₃)₂.3H₂O and Ni(NO₃)₂.6 H₂O salts were separately and at different molar ratios prepared at 0.2 M concentration in 40 ml distilled water. The solutions were prepared at different Ni substitution ratios of 0, 0.2, 0.4, 0.6, 0.8, and 1 as in form of Cu_{1-x}Ni_xO using magnetic stirrer. Diethanolamine was added gradually to each mixed solution of 0.84 g and mixed on a magnetic stirrer at room temperature. The pH was adjusted at 7 by adding some drops of HCl acid. After completing the dissolution process and obtaining the solution, thin films were immediately deposited on the previously cleaned glass substrates using spin coater at 1000 rpm and annealed at 500°C for 30 minutes to obtain metal oxide films.

Samples Characterization

The prepared Cu_{1-x}Ni_xO films at different ratios were examined by X-ray diffraction (PHILIPS PW 1840), Field emission scanning electron microscopy (MIRA3 TESCAN), Fourier transform infrared spectroscopy (FTIR) Spectroscopy (Shimadzu), and UV-visible absorption spectrometer (UV-1800).

Results and discussions

Figure 1. shows the XRD patterns of $Cu_{1-x}Ni_xO$ films at different ratios (x=0, 0.2, 0.4, 0.6, 0.8, and 1.0). All samples showed polycrystalline structure as the curves showed multiple diffraction peaks. These peaks appeared broad in appearance which indicates the nanostructure of the prepared samples. The pure sample showed two diffraction peaks at diffraction angle 2θ =35.39° and 38.74° which are attributed to the (11-1) and (111) crystallographic directions of the monoclinic CuO crystal structure according to the JCPDS standard card No. 96-410-5683. The replacement of nickel instead of copper and increasing the substitution ratio led to a gradual decrease in the intensity of these two peaks until disappear at x=0.8 ratio while a new phase begins to appear at this ratio corresponding to cubic structure of NiO. Two peaks appeared at 37.39° and 43.49° which are corresponding to the crystallographic directions (111) and (200) according to the JCPDS card No. 96-432-0488. The intensity of these two peaks increases with increasing nickel content which indicates an increase in the degree of crystallization of the sample. A slight shift in the locations of the peaks was noticed with changing the Ni content due to the strain resulting in the crystal lattice from the difference in the ionic diameter between the replaced and substituted ions.

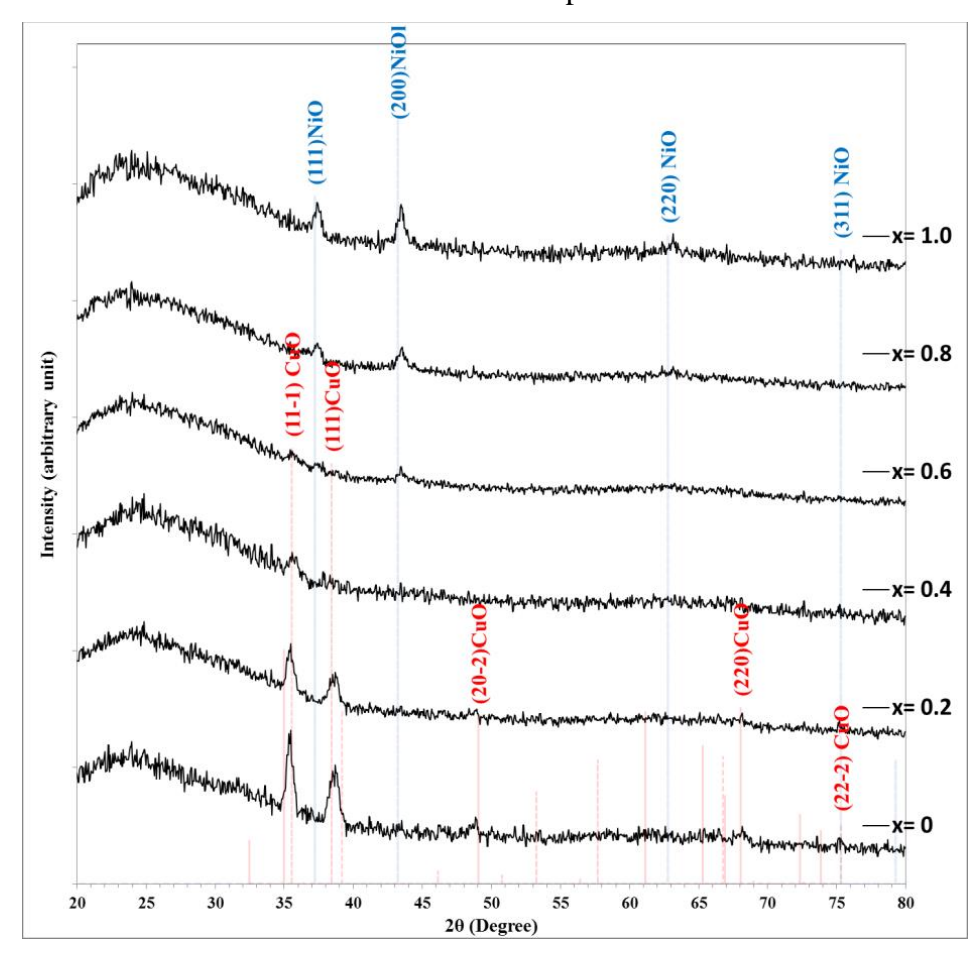


Figure 1. XRD patterns of Cu_{1-x}Ni_xO composite thin films at different ratios.

Figure 2. shows a two-dimensional representation of the XRD of Cu_{1-x}Ni_xO films using Xpowder software, which shows the phase transition point with the nickel compensation ratio. This figure

indicates that the CuO phase appears as a single phase in the pure sample and at low nickel content up to x=0.4. This is due to the fact that the added nickel ions penetrate into the copper oxide lattice as a substitution element instead of copper ions. This substitution leads to strain in the lattice, which appears in the form of a slight shift in the positions of the diffraction peaks, which is clearly evident between x values of 0.4 and 0.6 in the $(11\overline{1})$ direction. Increasing the nickel ion ratio greater than 0.6 led to a phase inversion to be the nickel oxide composition is dominant.

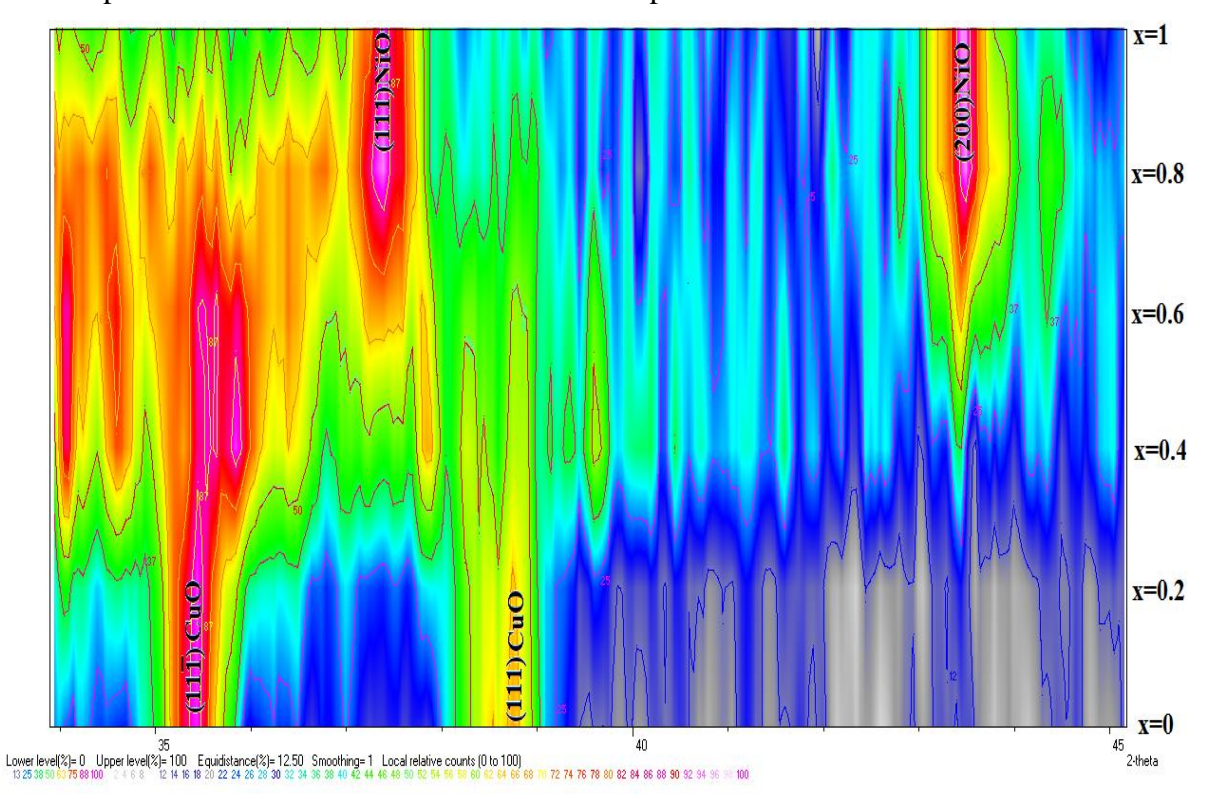


Figure 2. Two-dimensional representation of XRD of Cu_{1-x} Ni_xO thin films using Xpowder software showing the phase transformation with nickel element compensation.

The interplaner distances (d_{hkl}) were calculated using Bragg's equation [18]:

$$n \lambda = 2 d_{hkl} \sin \theta (1)$$

where θ is the Bragg diffraction angle, λ is the wavelength of the X-rays used for the copper target inside the X-ray generating tube and is equal to 0.15406 nm, and n is the diffraction order.

The crystallite size (D) was calculated using the Debye-Scherrer formula based on the full width at half maximum of diffraction lines intensity (FWHM) [19]:

$$D = \frac{0.9 \,\lambda}{FWHM.cos(\theta)} \,(2)$$

Table 1. lists the XRD results represented by the Bragg angles, FWHM, d_{hkl} and D. The calculated d_{hkl} values are very close to their values in the standard card. The difference in D values for two peaks in the same sample indicates the difference in growth in different directions. Increasing the nickel ratio in the sample leads to a decrease in the grain size of the copper oxide crystals until they disappear at the ratio x=0.6, while a greater increase in the nickel replacement shows an increase in the crystallite size of the nickel oxide crystals.

Table1. XRD parameters of Cu_{1-x}Ni_xO composite thin films at different ratios.

X	2θ (Deg.)	FWHM (Deg.)	d _{hkl} Exp.(Å)	D (nm)	hkl	Phase
0.0	35.39	0.5170	2.5343	16.1	(11-1)	Monoclinic CuO
	38.74	0.8490	2.3225	9.9	(111)	Monoclinic CuO
0.2	35.44	0.7170	2.5308	11.6	(11-1)	Monoclinic CuO
	38.74	0.8460	2.3225	10.0	(111)	Monoclinic CuO
0.4	35.84	1.8460	2.5035	4.5	(11-1)	Monoclinic CuO
	37.84	1.0100	2.3757	8.3	(111)	Monoclinic CuO
0.6	43.44	0.8330	2.0815	10.3	(200)	Cubic NiO
0.8	37.39	1.8630	2.4032	4.5	(111)	Cubic NiO
	43.49	0.7940	2.0792	10.8	(200)	Cubic NiO
1.0	37.39	1.1570	2.4032	7.3	(111)	Cubic NiO
	43.44	0.7000	2.0815	12.2	(200)	Cubic NiO

The surface structure of the samples has a significant effect on many physical properties. The morphology of the samples surface was examined within the nanoscale range using field effect scanning electron microscopy (FE-SEM). Figure 3-a, and b show the top-view images, at two magnifications, of the Cu_{1-x}Ni_xO thin films prepared with different compensation ratios. The pure copper oxide sample showed a porous structure formed by close interconnection between microstructures with dimensions of about 3 µm forming the general porous structure. The images with higher magnification showed nanoparticles with diameters ranging from 79 to 137 nm attached to the surface of the microparticles. The addition of nickel at a molar ratio of 0.2 led to a change in the surface structure of the sample where the compact structures appeared with smaller sizes with a diameter of about 1 µm with increased interconnection between the particles and decreased surface porosity. The image with higher magnification power shows cubic nanoparticles attached to the surfaces with side length of about 250 nm. Increasing the nickel ratio to 0.4 led to the particles being more compact with each other. The variation in the degree of compactness of the samples with changing the Ni content is due to the difference in the nature of the crystallization of the metals. This change in the general structure of the sample leads to a change in other properties such as optical properties. The thin film sample at the ratio x = 0.6 showed an extended surface consisting of stacked plate like structures containing some cavities. The deposited films also contain disk-like shapes fixed in random directions in the surface with nanoscale dimensions with a diameter of 93 nm and a thickness of 26 nm. Increasing the Ni ratio to x = 0.8 leads to an increase in the number of disk-like shapes per unit area, until they become highly dense. These disks have diameters of about 154 nm and a thickness of 20 to 25 nm. The disk-like belong to the nickel oxide structure, where many studies have shown the possibility of depositing doped nickel oxide in the form of nanodiscs [20,21]. Many applications depend heavily on the surface properties and composition of the nanostructure, where the sample meets the requirements of a large surface-tovolume ratio. This structure with a large surface area is preferred in gas sensor or photocatalyst applications [22,23]. The thin film sample at x=1 exhibited a regular, slightly porous extended surface consisting of spherical nanoparticles of almost uniform sizes with diameters ranging from 34 to 61 nm stuck together.

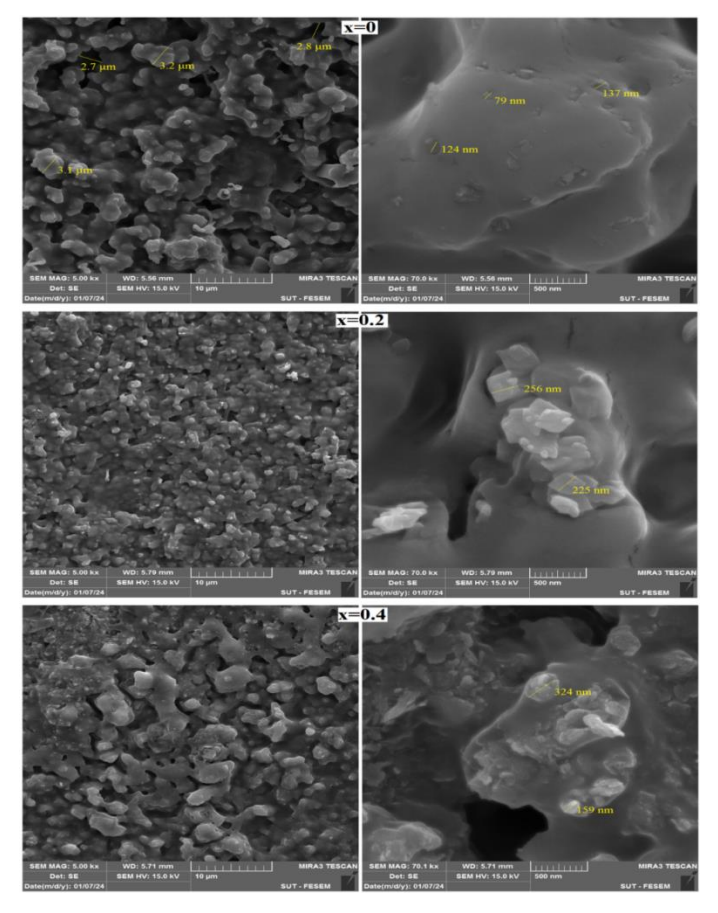


Figure 3 (a). Top-view SEM images of $Cu_{1-x}Ni_xO$ films at x ratios = 0, 0.2, and 0.4.

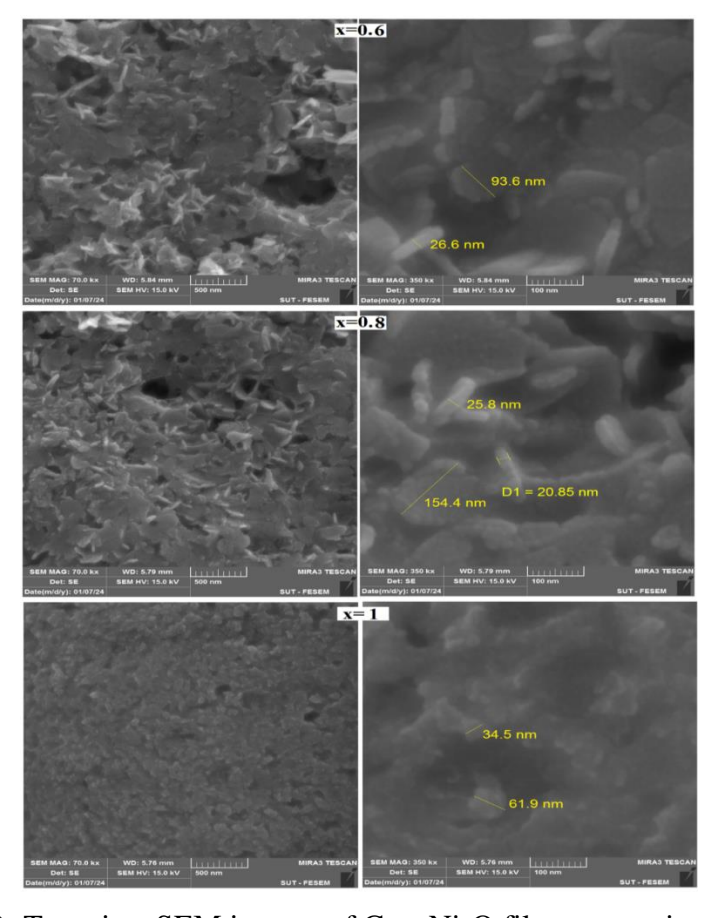


Figure 3 (b). Top-view SEM images of $Cu_{1-x}Ni_xO$ films at x ratios = 0.6, 0.8, 1.

Figure 4. illustrates the transmittance patterns of FTIR in the wavenumber range of 400 to 4000 cm⁻¹ for Cu_{1-x}Ni_xO films at different blending ratios. In the pure copper oxide sample, the sharp absorption peaks at 426 and 513 cm⁻¹ are attributed to the symmetric and asymmetric stretching vibrations of the Cu-O bond in the monoclinic copper oxide phase [24]. Additional absorption bands appeared in the curve, notably at 3548.18 cm⁻¹, which are due to the N-H stretching vibration from residual raw materials. The band at 3457.81 cm⁻¹ is due to the stretching vibration of the hydroxyl ion (O–H), while the band at 1767.13 cm⁻¹ is due to the bending vibrations in water molecules adsorbed on the surface of the sample. The band at 1635.95 cm⁻¹ is due to the N-H bond, 1382.35 cm⁻¹ to the C-H bond, 1047.13 cm⁻¹ to the C-O bond, and the bands at 880.97, 787.69, and 679.84 cm⁻¹ are due to the C-H bond [1]. These values, listed in Table 4.3, arise from the atmosphere or as residual materials in the sample from the raw materials [25].

Replacing the copper ion with the nickel ion and increasing the percentage of Ni led to a gradual decrease in the intensity of the peaks due to Cu-O until they disappeared, with broad bands appearing around wavenumbers 671.09 and 516.60 cm⁻¹ at the ratio x=0.6 and above, attributed to the vibrations of the Ni-O bond [26]. Differences in the intensity and locations of other peaks are due to fluctuations in the amount of adsorbed material on the surface, which depend on several factors such as the sample's porosity. The slight difference in the location of the bonds corresponding to copper oxide and nickel oxide indicates a slight decrease in bond energy, resulting from the difference in bond length caused by lattice strain from crystal defects.

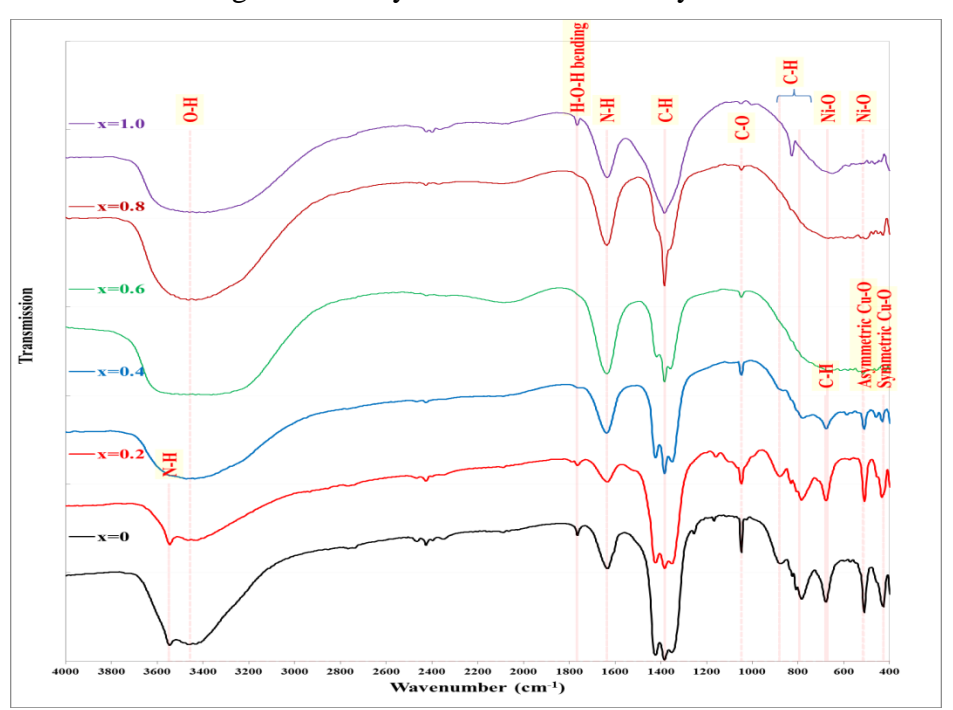


Figure 4. FTIR spectra of Cu_{1-x}Ni_xO thin films at different ratios.

Table 2: Bond types and energies in Cu_{1-x}Ni_xO thin films at different ratios.

Band Type	x=0	x=0.2	x=0.4	x=0.6	x=0.8	x=1.0
N-H	3548.18	3548.18	-	-	-	-
O-H stretch	3457.81	3443.24	3449.07	3437.41	3449.07	3434.49
H-O-H bending	1767.13	1764.21		-	-	1767.13
N-H	1635.95	1635.95	1635.95	1638.87	1638.87	1638.87
С-Н	1382.35	1385.26	1382.35	1385.26	1385.26	1388.18
C-O	1047.13	1050.04	1050.04	1050.04	1050.04	-
С-Н	880.97	880.97	880.97	-	-	828.50

	787.69	784.78	778.95	-	-	-
	679.84	679.84	676.92	-	1	-
Asymmetric Cu-O	513.68	512.77	510.68	-	1	-
Symmetric Cu-O	426.24	434.98	432.07	-	1	-
Ni O milanation	-	-	-	671.09	670.30	656.52
Ni-O vibration	1	-	-	516.60	504.94	481.62

The optical properties of thin films is a useful tool for determining the interaction of light with the material to determine the possibility of using them in optoelectronic applications such as solar cells and photodetectors. **Figure 5** shows the absorption spectra of Cu_{1-x}Ni_xO thin films deposited at different mixing ratios over the wavelength range from 300 to 1100 nm. In general, the absorbance decreases with increasing wavelength for all samples, which is a general characteristic of semiconductors, as only photons with energy greater than the energy gap (less than the critical wavelength) can generate electron-hole pairs. We notice that the absorption edge is located at approximately 350 nm for all samples, i.e. in the ultraviolet region. While the absorbance is very low (i.e. the transmittance is high) in the visible range. These films with high transmittance can be used as windows in solar cell applications [27]. The absorption spectra are affected by the components of the material and the nature of its composition. A decrease in absorbance can be observed with increasing the Ni content.

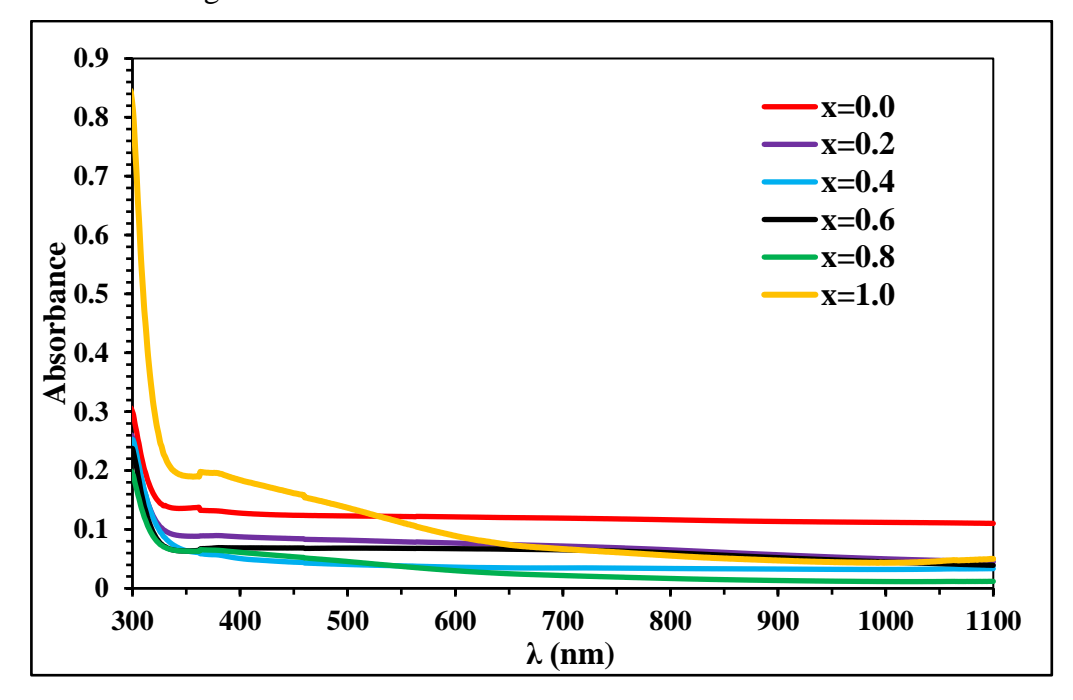


Figure 5. Absorption spectra variation of Cu_{1-x}Ni_xO thin films prepared at different ratios.

The optical energy gap of $Cu_{1-x}Ni_xO$ thin films prepared at different mixing ratios was calculated using Tauc's relation. This method involves plotting $(\alpha h v)^2$ against photon energy hv, as shown in **Figure 6**, where α , h, and v represent the absorption coefficient, Planck's constant, and light frequency, respectively. The point of intersection of the tangent with the x-axis represents the energy gap. A slight change in the optical energy gap values was observed, which gradually increased with increasing nickel substitution from 3.90 eV for the copper oxide sample to 3.98 eV for the nickel oxide sample. The slight difference in the energy gap is attributed to the variation in the material composition of the samples, with NiO thin films having a wide energy gap of up to 4 eV [28].

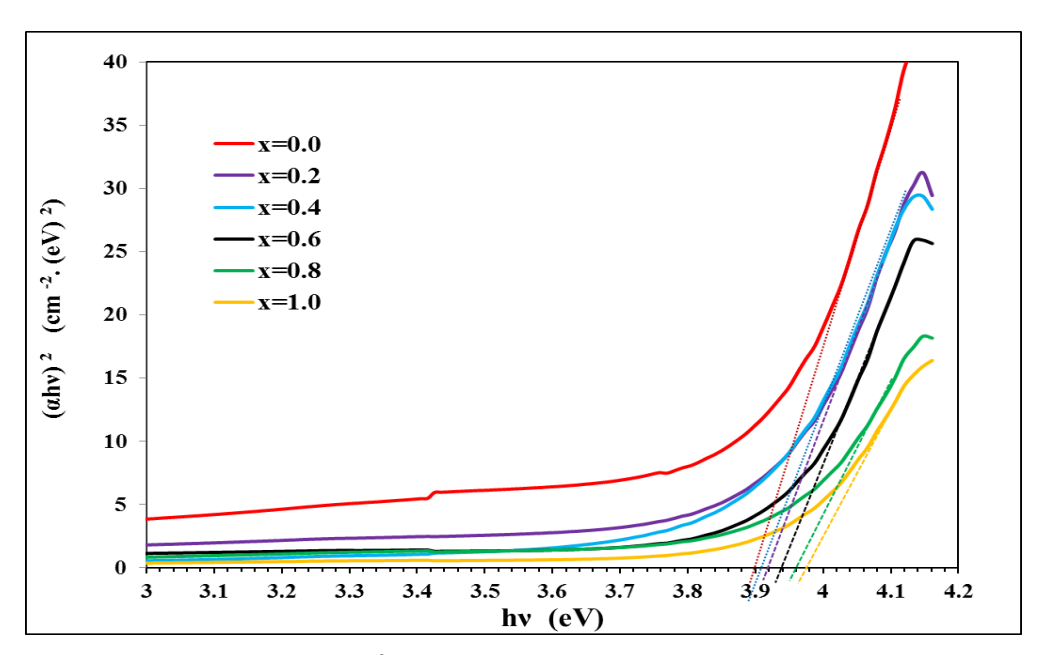


Figure 6. Relationship between $(\alpha hv)^2$ and hv for $Cu_{1-x}Ni_xO$ thin films prepared at different ratios.

Conclusions

The prepared Cu_{1-x}Ni_xO films with varying nickel substitution ratios using spin coating technique demonstrating significant structural and functional changes with increasing nickel content. The XRD results showed polycrystalline structures with a nano scale. The pure sample exhibited a monoclinic CuO structure, which gradually converted to the cubic NiO phase with increased nickel substitution. Scanning electron microscopy (SEM) revealed that the CuO film had a porous structure. The addition of nickel reduced particle size, increased connectivity, and decreased surface porosity. High nickel ratio films exhibited disc-shaped structures with nano dimensions. The EDX analysis indicated a lower content of oxygen, suggesting oxygen vacancies that are beneficial for catalytic activity. FTIR spectroscopy showed characteristic bands for nanocrystalline copper oxide, with nickel substitution resulting in the emergence of the Ni-O bands. Optical absorption studies showed the absorption edge around 350 nm for all samples, with high increasing transmittance up to 93% for NiO in the visible range, suggesting their suitability for solar cell applications. The optical bandgap slightly increased with nickel substitution. The high transmittance and large surface area of Cu_{1-x}Ni_xO films make them ideal for use in gas sensors, photocatalysts, and as window materials in solar cells, enhancing their efficiency and performance in these applications. Varying the nickel substitution ratios proved to be an effective way to tune the properties of the deposited films, allowing for precise control over their structural, optical, and catalytic characteristics. This method offers a useful approach to adjusting the films for specific applications.

References

- 1. M. Shaban, K. Abdelkarem, and A. M. El Sayed, Structural, optical and gas sensing properties of Cu2O/CuO mixed phase: effect of the number of coated layers and (Cr + S) co-Doping, Phase Transitions 92(4), 347–359 (2019).
- 2. E. Y. Salih, M. B. Ali Bashir, A. H. Rajpar, and I. A. Badruddin, Fabrication and characterization of porous Si/CuO film for visible light MSM photodetector: The effect of post-processing temperature, Ceramics International 48(7), 9965–9972 (2022).
- 3. A. K. Bhardwaj, V. Kumar, V. Pandey, R. Naraian, and R. Gopal, Bacterial killing efficacy of synthesized rod shaped cuprous oxide nanoparticles using laser ablation technique, SN Applied Sciences 1(11), 1426 (2019).
- 4. M. Balık, V. Bulut, and I. Y. Erdogan, Optical, structural and phase transition properties of

- Cu2O, CuO and Cu2O/CuO: Their photoelectrochemical sensor applications, International Journal of Hydrogen Energy 44(34), 18744–18755 (2019).
- 5. B. A. Aljurani, G. Y. Hermiz, and M. F. Alias, Superconductivity Measurements of (Hg,Tl)-1223 Compound Prepared in Capsule, Iraqi Journal of Science 2934–2939 (2021).
- 6. Muyang Shi, T. Qiu, B. Tang, G. Zhang, R. Yao, W. Xu, J. Chen, X. Fu, H. Ning, and J. Peng, Temperature-Controlled Crystal Size of Wide Band Gap Nickel Oxide and Its Application in Electrochromism, Micromachines (Basel) 12(1), 80 (2021).
- 7. A. K. Rai, L. T. Anh, C. Park, and J. Kim, Electrochemical study of NiO nanoparticles electrode for application in rechargeable lithium-ion batteries, Ceramics International 39(6), 6611–6618 (2013).
- 8. N. Rajput, Methods Of Preparation of Nanoparticles A Review, International Journal of Advances in Engineering & Technology 7(4), 1806–1811 (2015).
- 9. P. Sen, J. Ghosh, and A. Abdullah, Preparation of Cu, Ag, Fe and Al nanoparticles by the exploding wire technique, Proc. Indian Acad. Sci. (Chem. Sci.) 115, 499–508 (2003).
- 10. S. Dolai, R. Dey, S. Das, S. Hussain, R. Bhar, and A. K. Pal, Cupric oxide (CuO) thin films prepared by reactive d.c. magnetron sputtering technique for photovoltaic application, Journal of Alloys and Compounds 724, 456–464 (2017).
- 11. A. G. Ramu, M. L. A. Kumari, M. Soliman, H. H. Alkhamis, A. F. Alrefaei, and D. Choi, Chemosphere A facile and green synthesis of CuO / NiO nanoparticles and their removal activity of toxic nitro compounds in aqueous medium, Chemosphere 271, 129475 (2021).
- 12. S. Yousaf, S. Zul, M. Noureen, M. Farooq, N. F. Al-khalli, M. F. Aly, and I. Shakir, Tuning the structural, optical and electrical properties of NiO nanoparticles prepared by wet chemical route, (August), (2019).
- 13. E. Arulkumar, S. Thanikaikarasan, S. Rajkumar, and W. Wondimu, Influence of solution pH dependency on structure, optical with photoelectrochemical characteristics of SILAR deposited copper oxide thin films, Heliyon 10(13), e33579 (2024).
- 14. X.-H. Liu, X.-L. Jia, Y.-L. Zhao, R.-X. Zheng, Q.-L. Meng, C.-P. Liu, W. Xing, and M.-L. Xiao, Recent advances in nickel-based catalysts for electrochemical reduction of carbon dioxide, Advanced Sensor and Energy Materials 2(3), 100073 (2023).
- 15. M. Ben Arbia and E. Comini, Growth Processing and Strategies: A Way to Improve the Gas Sensing Performance of Nickel Oxide-Based Devices, Chemosensors 12(3), 45 (2024).
- 16. S. Biswas, Y. Saha, I. Mondal, D. Mondal, and M. Kundu, Synergistic approach for enhancement of optical and electrical dielectric properties of size-tunable Cu doped NiO semiconductor quantum nanoflakes Synergistic approach for enhancement of optical and electrical dielectric properties of size-tunable Cu dope, Current Applied Physics 56, 66–78 (2023).
- 17. Z. U. Rahman, U. Shah, A. Alam, Z. Shah, K. Shaheen, S. B. Khan, and S. A. Khan, Photocatalytic degradation of cefixime using CuO-NiO nanocomposite photocatalyst, Inorganic Chemistry Communications 148, 110312 (2023).
- 18. M. A. Kadhim, M. O. Salman, and A. A. Ramadhan, Effect of adding graphene on structural, surface morphology and optical properties of ZnO:SnO2 composite, AIP Conf. Proc. 2547, 030007 (2022).
- 19. M. Shafiey Dehaj and M. Zamani Mohiabadi, Experimental study of water-based CuO nanofluid flow in heat pipe solar collector, Journal of Thermal Analysis and Calorimetry 137(6),

- 2061–2072 (2019).
- 20. P. H. Suman, A. A. Felix, H. L. Tuller, J. A. Varela, and M. O. Orlandi, Comparative gas sensor response of SnO2, SnO and Sn3O4 nanobelts to NO2 and potential interferents, Sensors & Actuators: B. Chemical 208, 122–127 (2015).
- 21. M. J. Dathan, B. F. Hassan, Q. A. Abduljabbarb, and J. M. Rzaij, Nickel oxide doping impact on the NO2 sensing properties of nanostructured zinc oxide deposited by spray pyrolysis, Digest Journal of Nanomaterials and Biostructures 18(4), 1159–1167 (2023).
- 22. M. Poloju, N. Jayababu, and M. V. R. Reddy, Materials Science & Engineering B Improved gas sensing performance of Al doped ZnO / CuO nanocomposite based ammonia gas sensor, Materials Science & Engineering B 227(October 2017), 61–67 (2018).
- 23. E. N. Monitoring, R. Sasikala, K. Karthikeyan, E. Deivanayagam, and I. M. Bilal, Photocatalytic degradation of trypan blue and methyl orange azo dyes by cerium loaded CuO nanoparticles, Environmental Nanotechnology, Monitoring & Management (July), (2016).
- 24. A. I. Journal, M. Khatamifar, and S. J. Fatemi, Green synthesis of pure copper oxide nanoparticles using Quercus infectoria galls extract, thermal behavior and their antimicrobial effects, Particulate Science and Technology 0(0), 1–9 (2021).
- 25. M. S. Lashkenari, M. Ghorbani, H. Naghibi, and P. Khalaj, Synthesis and characterization of polyrhodanine/ nickel ferrite nanocomposite with an effective and broad spectrum antibacterial activity, POLYMER-PLASTICS TECHNOLOGY AND MATERIALS 58(13), 1–10 (2019).
- 26. S. D. Khairnar and V. S. Shrivastava, Facile synthesis of nickel oxide nanoparticles for the degradation of Methylene blue and Rhodamine B dye: a comparative study, Journal of Taibah University for Science 13(1), 1108–1118 (2019).
- 27. A. H. Jabbar, Fabrication and Characterization of CuO:NiO Composite for Solar Cell Applications, Journal of Advanced Research in Dynamical and Control Systems 24(4), 179–186 (2020).
- 28. M. Shi, T. Qiu, B. Tang, G. Zhang, R. Yao, W. Xu, J. Chen, X. Fu, H. Ning, and J. Peng, Temperature-Controlled Crystal Size of Wide Band Gap Nickel Oxide and Its Application in Electrochromism, Micromachines 12(1), 80 (2021).